

# VELOCITY STRUCTURE IN LONG PERIOD VARIABLE STAR ATMOSPHERES

C. Pilachowski and G. Wallerstein  
University of Washington  
Seattle, Washington

L. A. Willson  
Iowa State University  
Ames, Iowa

## ABSTRACT

A regression analysis of the dependence of absorption line velocities on wavelength, line strength, excitation potential, and ionization potential is presented, and conclusions are drawn regarding the velocity structure of the atmosphere and the regions of formation of different lines.

## I. MOTIVATION

### A. Observational Considerations and Method.

High dispersion absorption line spectra of long period (Mira) variables show much larger velocity scatter ( $\sim 5-8$  km/s) than similar quality observations of more normal M giants ( $\sim 1-2$  km/s, approaching the expected velocity resolution of the plates used in this study).

Previous investigators have noticed correlations between the velocity of absorption lines and the excitation potential of the lower levels (see for example Merrill, 1964a,b for U Ori, R Ser, R Hya; Adams 1941 and Joy 1954 for  $\alpha$  Ceti; Merrill 1952 for T Cas, R LMi, W Hya and T Cep). Preliminary inspection of the plates in the present study suggested the possibility of a strong correlation with ionization potential also for some of the plates.

For any atmosphere with a velocity gradient in the reversing layer the velocity determined from a given spectral line will depend on the equivalent width or line strength which determines the region of formation of the line. Maehara (1971) found a fairly strong dependence of the velocity of absorption lines on the line intensity for  $\chi$  Cyg. In addition, if the continuum opacity is strongly wavelength dependent, then one might hope to discover a correlation between the wavelength of the line and its velocity.

The present study is therefore an attempt to understand the systematic effects on the absorption line velocities of the four parameters excitation potential ( $\chi_e$ ), ionization potential ( $\chi_i$ ), line strength (S), and wavelength ( $\lambda$ ). For line strength a visual estimate on an integer

scale where most measured lines fall between 1 (very weak) and 4 (strong) has been used. The procedure has been to solve for coefficients in a multiple linear regression (least squares fit) with the four independent variables:

$$v = C_o + C_{f(\lambda)} \cdot f(\lambda) + C_s \cdot S + C_i \cdot \chi_i + C_e \cdot \chi_e \quad (1)$$

When a group of lines contains a wide spread of parameter values, such as excitation potentials from 0 eV to 3.5 eV or wavelength from 3800 Å to 4400 Å, then the correlation coefficients derived are not very sensitive to small errors in  $v$ . If the group contains only lines with similar parameter values, such as ionization potentials from 7.4 eV to 7.9 eV or wavelengths from 4000 Å to 4075 Å, then small errors in  $v$  lead to large variations in the coefficients. For this reason, as well as to reduce everything to a common set of velocity units to facilitate comparisons between coefficients, we tabulate the results in terms of parameter ranges  $X_R$  defined by

$$X_R = C_X (X_{\max} - X_{\min}) \quad (2)$$

where  $C_X$  is the coefficient for parameter  $X$ ,  $X_{\max}$  the maximum value assumed by the parameter in the sample, and  $X_{\min}$  the minimum value assumed. Note that for wavelength we have allowed for the use of functions of  $\lambda$ ; correlations have been calculated for  $f(\lambda) = \lambda$ ,  $1/\lambda$ ,  $1/\lambda^2$ , and  $1/\lambda^4$ . In general there were no differences in the results between  $f(\lambda) = \lambda$  and  $f(\lambda) = \lambda^{-4}$ , with a very slight improvement in the significance of the fit as  $f(\lambda)$  was changed from  $\lambda$  to  $1/\lambda$ ,  $1/\lambda^2$ , and  $1/\lambda^4$  in a few cases. We have therefore chosen to tabulate coefficients in terms  $1/\lambda$  as an intermediate "standard case".

We expect some relationships to hold between the signs of the four coefficients based on simple arguments. The ionization potential and excitation potential dependence should reflect the velocity as a function of distance from the source of excitation and ionization; the simplest models are therefore expected to have excitation potential coefficients and ionization potential coefficients of the same sign ( $C_i \cdot C_e > 0$ ). If the continuum opacity decreases from  $\sim 3600 \text{ \AA}$  to  $\sim 7800 \text{ \AA}$  (for example if the principal opacity source is Rayleigh scattering  $\propto \lambda^{-4}$ ) then lines in the blue region of the spectrum will be formed at higher atmospheric levels than will the lines in the red region. Also, strong lines are formed higher in the atmosphere than weak ones. Hence the coefficients in  $\lambda$  and  $S$  should have opposite signs, or those in  $1/\lambda$  and  $S$  the same sign ( $C_\lambda \cdot C_s < 0$  or  $C_{1/\lambda} \cdot C_s > 0$ ). Table 1 summarizes the four expected configurations based on these arguments, and the simplest general interpretation of each case.

B. Theoretical motivation and shock model interpretation.

The interpretation of emission lines in long period variable stars as produced in a moderately strong shock front rising from the photosphere once each cycle has proven very effective in interpreting those features (Willson 1976; Willson and Hill 1976) and is also confirmed by infrared observations (Hinkle 1978). A schematic velocity profile of a simple model for the shocked atmosphere (from Hill and Willson 1978) is shown in Figure 1. Important features of the models for the present study are:

1. The atmosphere typically contains two shocks. The lower shock, of large amplitude, produces the hydrogen emission lines and the visual continuum; the upper shock is in the reversing layer and is the direct cause most of the observed scatter in the velocities of the absorption lines.

2. The amplitude of the upper shock is expected to be  $\sim 10-20$  km/s for stars with masses  $\sim 1 M_{\odot}$  and periods from  $150^d$  to  $350^d$ .

3. The magnitude of the inward preshock velocity at a given shock is  $\geq$  the magnitude of the outward postshock velocity for the zero mass loss strictly periodic case.

Note that in a few cases the absorption lines in the red have been observed to be split, with components differing in velocity by typically 10-20 km/s (Shinkawa 1973 for S Car; Maehara 1971, for  $\chi$  Cyg and  $\alpha$  Ceti; present study plates DA0 7641 (RT Cyg) and EC 2688 (Z Oph)).

In Figure 1 we have also included an idealized distribution of velocities for A) Circumstellar lines, B and F) 0-1.0 eV lines, C and E) 1-3 eV lines, C) absorption lines of ionized elements, D) emission lines of ionized metals, and H) emission lines of hydrogen. This idealized distribution is based mainly on the results of the present study which indicate typical regions of line formation in the shock wave model for each of these classes of lines.

An interpretation of the coefficients of the regression analysis (cases a-d of Table 1) using the velocity profile of Figure 1 is presented in Table 2. There are two possible interpretations of cases c and d with the shock model, with different corollary behavior expected

as noted in the table. Isothermal hydrodynamic calculations (Willson and Hill 1976, Hill and Willson 1978) suggest a reasonable likelihood of a small region of increasing outward velocity behind the shock, as in case c1. There is, however, no very strong theoretical justification of a similar region of decreasing inward velocity ahead of the shock (case d1) although Hall (1978) sees a "hook" in the velocity of the high excitation components of molecular lines in the infrared vs. time that may result from such a decrease. In the present study the corollary behavior of the case d results strongly favors the second interpretation, unresolved splitting of low excitation lines, as does the fact that case d and mixed cases c, d account for a majority of the plates. Also in one case (DAO 7641) where the splitting is resolved, omitting the red components of the doubled lines converts this case d into a clear post shock case b.

Internal consistency for the regression analysis was judged on the basis of the following criteria:

1. Is the result a permitted model (one of cases a-d), i.e. physically reasonable?
2. Does the velocity distribution satisfy the "corollary behavior" of Table 2?
3. Does the exclusion or inclusion of an arbitrary set of lines leave the result unchanged?
4. Does the set of all regression fits satisfy our expectations for the simplest models ( $C_i \cdot C_e > 0$  and  $C_{1/\lambda} \cdot C_s > 0$  or cases a-d)?

Plots of the ranges of  $1/\lambda$  vs.  $S$  and of  $\chi_1$  vs.  $\chi_e$  for all the plates are shown in Figures 2 and 3. The "forbidden regions" have been shaded beyond the minimal error of 2 km/s from each axis. Error bars on each point are pre-fit standard deviations. Clearly the plates do generally satisfy the fourth consistency criterion. The few exceptions for Z Oph are red plates which turn out to have lines present representing both shocks, and for which our simple cases therefore do not apply.

In Figures 4 and 5 are plotted the coefficient ranges  $1/\lambda$  vs.  $\chi_1$  and  $S$  vs.  $\chi_e$ , with error bars as in Figures 2 and 3. The quadrants are marked according to the case each represents. The expected corollary behavior of small scatter plus small coefficients is seen for the pre-shock case a. For cases c and d large scatter and large coefficient ranges are both found - this is the corollary behavior expected if c and d both represent mixtures of lines from both sides of the shock.

The sensitivity of the results to the inclusion or exclusion of a few lines was investigated both through a series of calculations made deleting successively the most deviant lines in the sample (ones most likely to be misidentified, for example, with very high excitation or very high residual velocity) and through a "running solution". The running solution was a calculation of coefficients for sequential groups of ten lines. In Figure 6 the coefficient ranges for a running solution for S Car (D 895) are shown as a function of the average wavelength for the ten lines. Each successive group of ten lines includes five lines from the previous set. The conclusion suggested by our criteria regarding coefficient ranges and standard deviations, namely that the coefficients for  $\chi_1$  and  $\chi_e$  are the only ones which are significant, is clearly

supported by the trends in the running solution. The coefficients which the general analysis suggests are not significant show mostly a random scatter about zero.

The running solution is not only useful as a consistency check, it is also an efficient means of locating misidentified lines. Such lines generally cause an abrupt change in the coefficient ranges in the running solutions. In the example for S Car such "deviant" lines near 4500 Å may explain the overall lack of correlation for S even though most of the 10 point S coefficients are negative. There are in this case no obviously bad lines, however, so we have chosen to consider  $C_S$  not significant.

Note however that the running solution is a very poor means of checking the wavelength coefficient, since for lines listed in order of  $\lambda$  the wavelength interval for each set of ten lines is much smaller than the overall wavelength interval. For this reason a further check of the wavelength coefficient was made for those dates where two plates in different wavelength regions were available by calculating a single set of regression coefficients for these plates. In cases (such as DAO 10157 and 10162 of RT Cyg) where lines in both wavelength regions appear to be formed on the same side of the shock, the wavelength coefficients for the combined plates are consistent with those for each plate taken separately. For pairs of plates (such as Pc 3237 and 3238 of Z Oph) where there is clear evidence that the lines are formed on different sides of the shock, the combined plates create a very strong apparent wavelength dependence and yield a strong case d -- further evidence in favor of the cross shock interpretation for the case c and d results.

## II. ANALYSIS OF THE OBSERVATIONAL MATERIAL

In order to interpret the actual data in terms of the schematic models of Section I we must first develop criteria for the significance or lack of significance of the coefficients, and means of evaluating the regression fits for validity. Two approaches have been used: requiring internal consistency plus comparison with a "null" case, plate DAO 10936 of  $\beta$  Peg, with minimal observed scatter and for which velocity gradient effects are not expected.

The requirements for a significant fit can be summarized as follows:

1. No fit for fewer than 10 lines can be considered significant.

2. The fit must significantly decrease the scatter. Mathematically we insist that

$$SD^f / SD^o \leq .9$$

where  $SD^o$  is the standard deviation of the observed velocities in the sample and  $SD^f$  is the standard deviation for the differences between observed and predicted (from the regression fit) velocities for each line in the sample. Ideally this requirement should be written in terms of a function of  $n$ , the number of lines in the sample. However, after samples containing less than 10 lines have been eliminated, and considering the relatively limited typical sample sizes (25-100 lines) used here, the constant .9 should suffice.

3. A coefficient in the regression fit is deemed significant if and only if the range for that coefficient is greater than the original standard deviation  $SD^o$ :

$$X_R \geq SD^o . \quad (4a)$$

The coefficient is marginally significant if

$$X_R \geq SD^f . \quad (4b)$$

In Table 3 the results of the regression for one plate each of  $\beta$  Peg,  $L^2$  Pup and S Car, for 8 plates of RT Cyg, and for 7 plates of Z Oph are summarized. Those coefficients which satisfy Equation 4a are underlined with a solid line; those which satisfy Equation 4b are underlined with a dashed line; coefficients without underlining are not significant.

Reassuringly,  $\beta$  Peg is found to contain no significant velocity correlations by our criteria. The case from Tables 1 and 2 which best describes each plate is listed in Table 3 also; parentheses and double assignments are used for cases which do not satisfy criterion 2 or where only one of the coefficients is significant by Equation 4a.

An immediately striking result is the large number of d and c,d results for plates with fairly large scatter. In an attempt to further clarify the interpretation of these cases, to distinguish between the two possible interpretations suggested in Table 2, we have plotted histograms of velocity for various groups of lines: low excitation (0-1 eV) absorption lines (0), moderate excitation (1-3 eV) absorption lines (X), high excitation (>3 eV) absorption lines (+), absorption lines of ions (II), emission lines of neutral atoms other than H (Fe, Cr, etc.) and ions (EII), and emission lines of hydrogen (H,H'). Such plots are shown in Figures 7 to 12 for  $\beta$  Peg,  $L^2$  Pup, S Car, RT Cyg at maximum (DAO 10157, 10162) and at +33/34<sup>d</sup> (DAO 7631, 7641) and Z Oph at +47<sup>d</sup> (Pc 3237, 3238). These particular examples were selected as those

which most clearly illustrate the interpretation of several different cases with the shockwave model.

For  $\beta$  Peg (DAO 10936, Figure 7) we find a nearly Gaussian distribution with small scatter, mostly low excitation lines ( $n(1-3 \text{ eV})/n(0-3 \text{ eV}) = .35$  and no lines with  $\chi_e > 3 \text{ eV}$ ) and no emission lines. This agrees with our expectation that  $\beta$  Peg does not have extensive velocity gradients, and suggests that our method produces significant results only for stars which are truly "abnormal".

The histogram of velocities for  $L^2$  Pup (Figure 8) suggests that most of the lines are formed above the shock. The most probably stellar velocity is  $\sim 53 \text{ km/s}$  giving pre-shock infall velocity  $\sim 5 \text{ km/s}$  and post-shock outward velocity also  $\sim 5 \text{ km/s}$ . The lower shock (from the emission lines of H and Si) is near  $\sim 40 \text{ km/s}$ , i.e., rising with velocity relative to the star  $\sim 13 \text{ km/s}$ .

For S Car (Figure 9) the interpretation is less straightforward. From the location of the H emission lines the lower shock post shock velocity appears to lie  $280 \text{ km/s}$ ; from the absorption lines of the ions there appears to be preshock infalling material at  $\sim 300 \text{ km/s}$ . There are peaks in low excitation at  $288 \text{ km/s}$  (= most likely stellar velocity?) and  $\sim 291 \text{ km/s}$  and peaks in 1-3 eV lines around  $283 \text{ km/s}$  and  $294 \text{ km/s}$ . Following the notation of Figure 1 it seems likely that we are seeing both shocks, with velocities A =  $288 \text{ km/s}$ , C =  $294 \text{ km/s}$ , D =  $283 \text{ km/s}$ , G =  $300 \text{ km/s}$  and H =  $280 \text{ km/s}$ . This means outward velocities relative to the star of  $5 \text{ km/s}$  (upper shock) and  $8 \text{ km/s}$  (lower shock), inward velocities of  $6 \text{ km/s}$  and  $12 \text{ km/s}$  for the two shocks, or total shock

amplitudes of 11 km/s and 20 km/s for the two shocks. This is in exact agreement with Shinkawa (1973) who found velocity curve amplitudes of 11 km/s (visual) and 20 km/s (infrared).

A common feature of all the velocity histograms is the concentration of the absorption lines of certain ions on the red edge of the main velocity peak. The interpretation of this was suggested by Figure 2: these lines are probably formed in the region immediately ahead of the shock where radiative ionization of Ba, Sr, Sc, etc. has taken place. These lines are then the best indicators of the limiting infall velocity of the material ahead of the shock.

In Figures 10-12 the velocities A-H have been indicated as far as it is possible to locate them. For RT Cyg near maximum both the red plate (DAO 10157) and the blue plate (DAO 10162) give the same mean absorption line velocity, the same scatter, and the similar ratios of low excitation to high excitation lines, suggesting both show lines from the same region. The red plate includes one possible split line, VI(19)  $\lambda$  6292, with  $\Delta v = 15$  km/s which may be the amplitude of the upper shock. The red component of this line agrees with the absorption lines of ions (in DAO 10162) in placing the pre-shock infall velocity (C) near -109 km/s. The emission line velocities from hydrogen are particularly unreliable near maximum, when overlying absorption is strongest, but all the lines together suggest the existence of shocks with post shock velocities  $D \approx -125$  km/s and  $H \approx -131$  km/s.

Figure 11 shows the clearest case of resolved line splitting, plate DAO 7641 of RT Cyg at  $34^d$ , with the blue plate DAO 7631 taken one day

previously. There clearly are two groups of velocities peaking near -113 km/s and -128 km/s. In Table 3 two analyses of 7641 are listed: one for a set of velocity measurements made with a single average velocity used for the split lines (7641 A) and one set of measurements (7641 B), plotted in Figure 12, which includes separate determinations for each component. The first determination yielded case d2 (unresolved doubling, large scatter); this became case b (post shock region) when the red components of the doubled lines were excluded from the fit. This pair of plates thus provides dramatic confirmation of the shock interpretation of the regression coefficients for the absorption line velocities.

A final very interesting pair of consecutive plates of Z Oph are shown in Figure 12. Pc 3237 is a red plate ( $\lambda\lambda$  5567-6707 Å) and Pc 3238 is a blue plate (4156-4571 Å) both taken at phase +47<sup>d</sup>. In the red we are clearly seeing below the shock, with a preponderance of high excitation lines, large scatter, and  $\langle v \rangle = -93$  km/s or net outward velocity (based on an estimated stellar velocity of -85 km/s) of  $\sim 8$  km/s. The lines in the blue plate, on the other hand, clearly originate above the shock, with more low excitation lines, less scatter, and  $\langle v \rangle = -80$  km/s suggesting infall velocity  $\sim 5$  km/s. Confirmation here also comes from the "anomalous" absorption and emission lines in the blue plate, which extend past the mean velocity of the red plate.

In Table 4 we summarize some known properties of the four long period variable stars in this study, with the shock amplitudes and stellar velocities suggested by the present analysis. For these four

stars, within the accuracy of the present analysis, the amplitude of the reversing layer shock near maximum light appears to be  $15 \pm 5$  km/s, with no obvious dependence on period or spectral type.

### III. GENERAL CONCLUSIONS

The scatter which is frequently found in velocity measurements of absorption lines in long period variables is probably the result of a shock of moderate amplitude (10-20 km/s) located in or near the reversing layer. The frequently observed correlations of velocity with excitation and ionization potential are a result of the velocity gradients produced by this shock in the atmosphere. A straight-forward linear regression analysis with parameters  $\lambda$ ,  $S$ ,  $\chi_e$ , and  $\chi_i$  is an effective way of determining the region of formation of the absorption lines for a given date and wavelength region. We have presented here a simple interpretation of the signs of the coefficients of the regression analysis in terms of case a: preshock; case b: post shock; cases c or d: across the shock, together with criteria for evaluating the validity of the fit. Finally, careful analysis of a series of plates for four long period variable stars has allowed us to estimate the amplitude of the reversing layer shock and also the most probable stellar velocity for these stars (Table 4). The results are in substantial agreement with previous velocity observations where such are available.

## ACKNOWLEDGEMENTS

We are pleased to acknowledge the assistance of the Directors of these observatories: Dominion Astrophysical Observatory, Hale Observatories, Cerro Tololo Interamerican Observatory, and Lick Observatory, for the use of their telescopes and spectrographs, as well as the Astronomy Department of the California Institute of Technology for use of the Grant measuring engine. This research was supported by grants from the National Science Foundation.

## BIBLIOGRAPHY

- Adams, W. S., 1941, Ap. J. 93, 19.
- Campbell, L., 1955, Studies of Long Period Variables, AAVSO, Cambridge, MA.
- Clayton, M. L. and Feast, M. W., 1969, MNRAS 146, 411.
- Feast, M. W., 1963, MNRAS 125, 367.
- Hall, D., 1978, (private communication).
- Hill, S. J. and Willson, L. A., [in preparation].
- Hinkle, K., 1978, Ap. J. 220, 210.
- Joy, A. H., 1954, Ap. J. Suppl 1, 39.
- Kukarkin, B. V. et al., General Catalogue of Variable Stars, Moscow, 1,  
1958, 2, 1965, 3, 1971.
- Maehara, H., 1968, PASJ 20, 77.
- Maehara, H., 1971, PASJ 23, 503.
- Merrill, P. W., 1964a, Ap. J. 102, 348.
- Merrill, P. W., 1964b, Ap. J. 103, 6.
- Merrill, P. W., 1952, Ap. J. 116, 18.
- Merrill, P. W., and Greenstein, J. L., 1958, PASP 70, 98.
- Shinkawa, D., 19 , Ap. J. Suppl. 25, 253.
- Willson, L. A., 1976, Ap. J. 205, 172.
- Willson, L. A. and Hill, S. J., 1976, Stellar Pulsation Conference  
(Los Alamos Scientific Laboratory) p. 279.

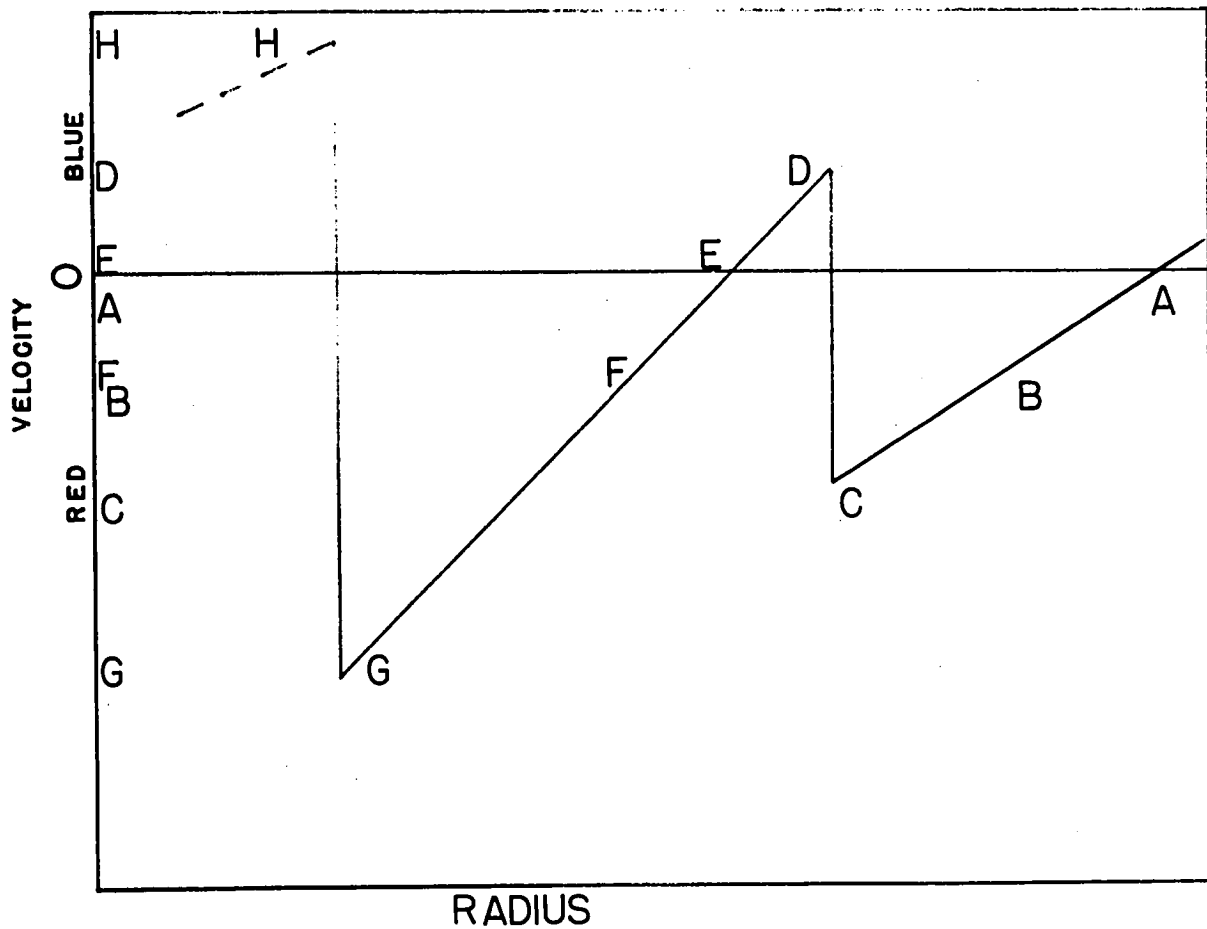


Figure 1. Schematic shock structure and regions of line formation: A, stellar velocity; B to C: increasing excitation pre shock velocities; D: post shock velocity; D to E or F: decreasing excitation; G: higher excitation pre shock region for the lower shock; H: rising post shock region, hydrogen emission line formation.

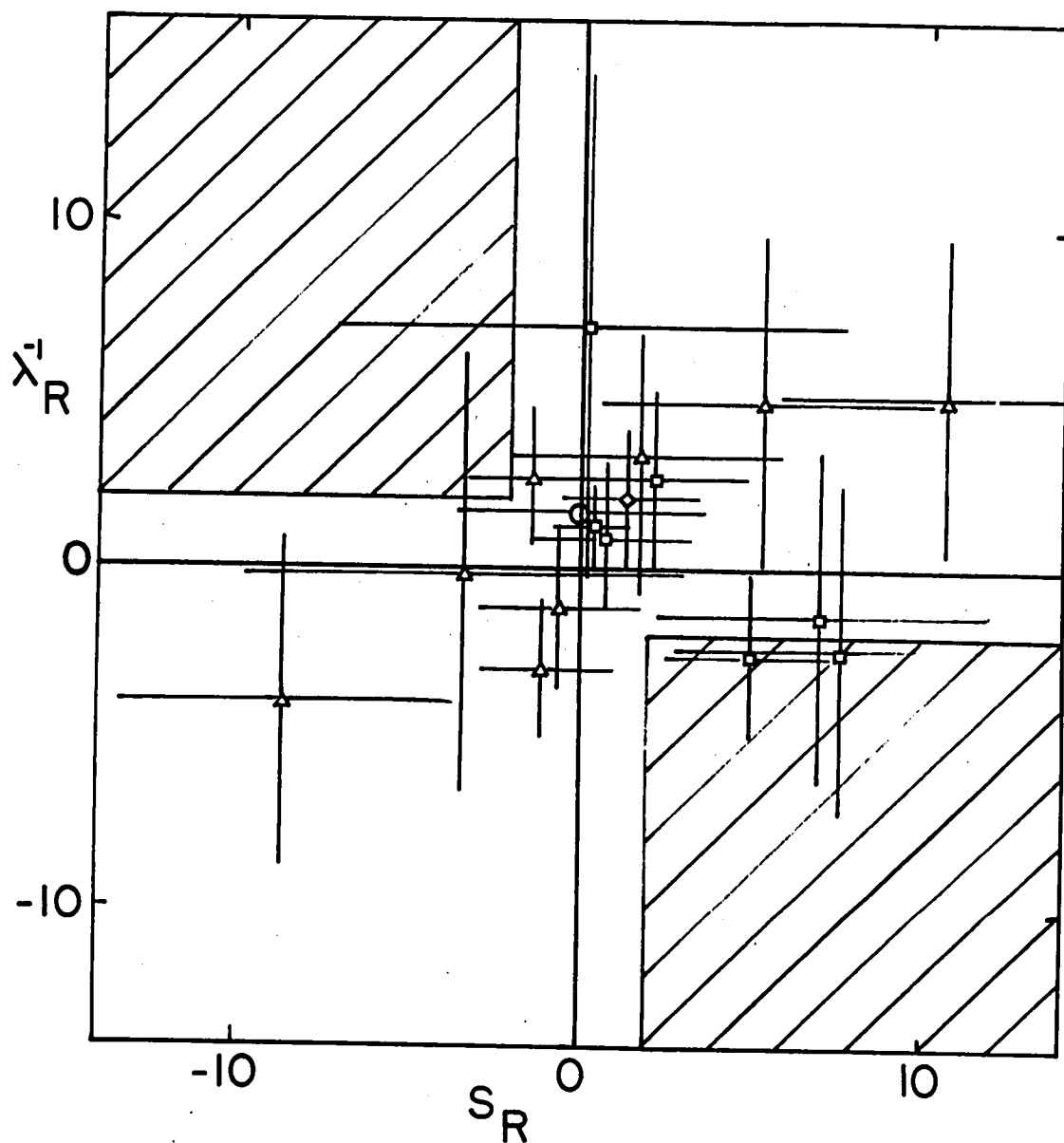


Figure 2. Plot of range of  $1/\lambda$  coefficient vs. range of S coefficient for RT Cyg ( $\Delta$ ), Z Oph ( $\square$ ), S Car ( $\circ$ ), and  $L^2$  Pup ( $\diamond$ ). Error bars are standard deviations of observed velocities. Shaded region is forbidden region according to cases a-d of Table 1 and assuming a residual scatter of  $\sim 2$  km/s.

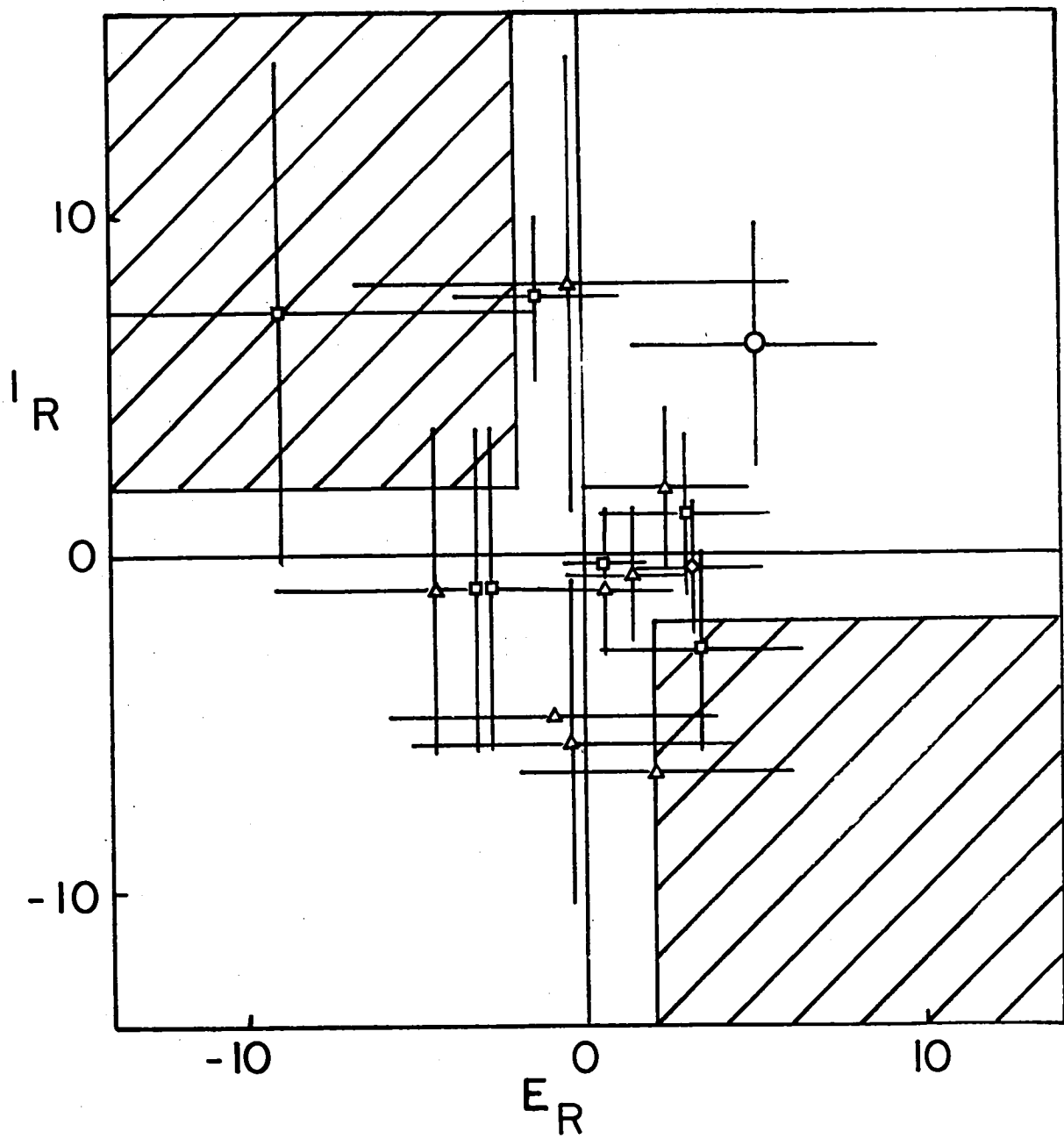


Figure 3. Coefficient ranges for  $x_1$  vs.  $x_e$ . Symbols and shading as for Figure 2.

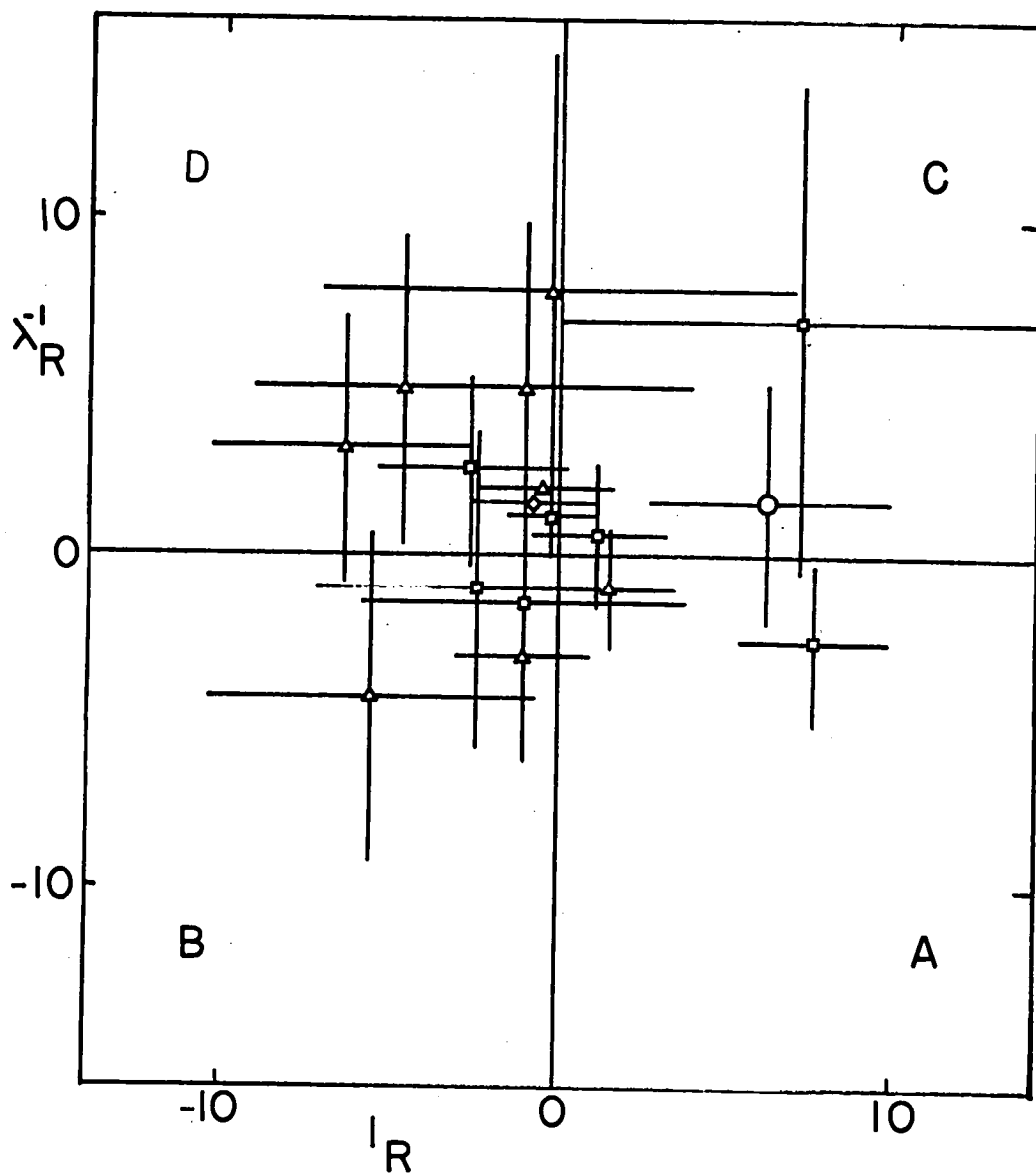


Figure 4. Coefficient ranges for  $1/\lambda$  vs.  $\chi$ ; symbols as in Figures 1 and 2. Each quadrant represents one case of Table 1 and is labelled accordingly.

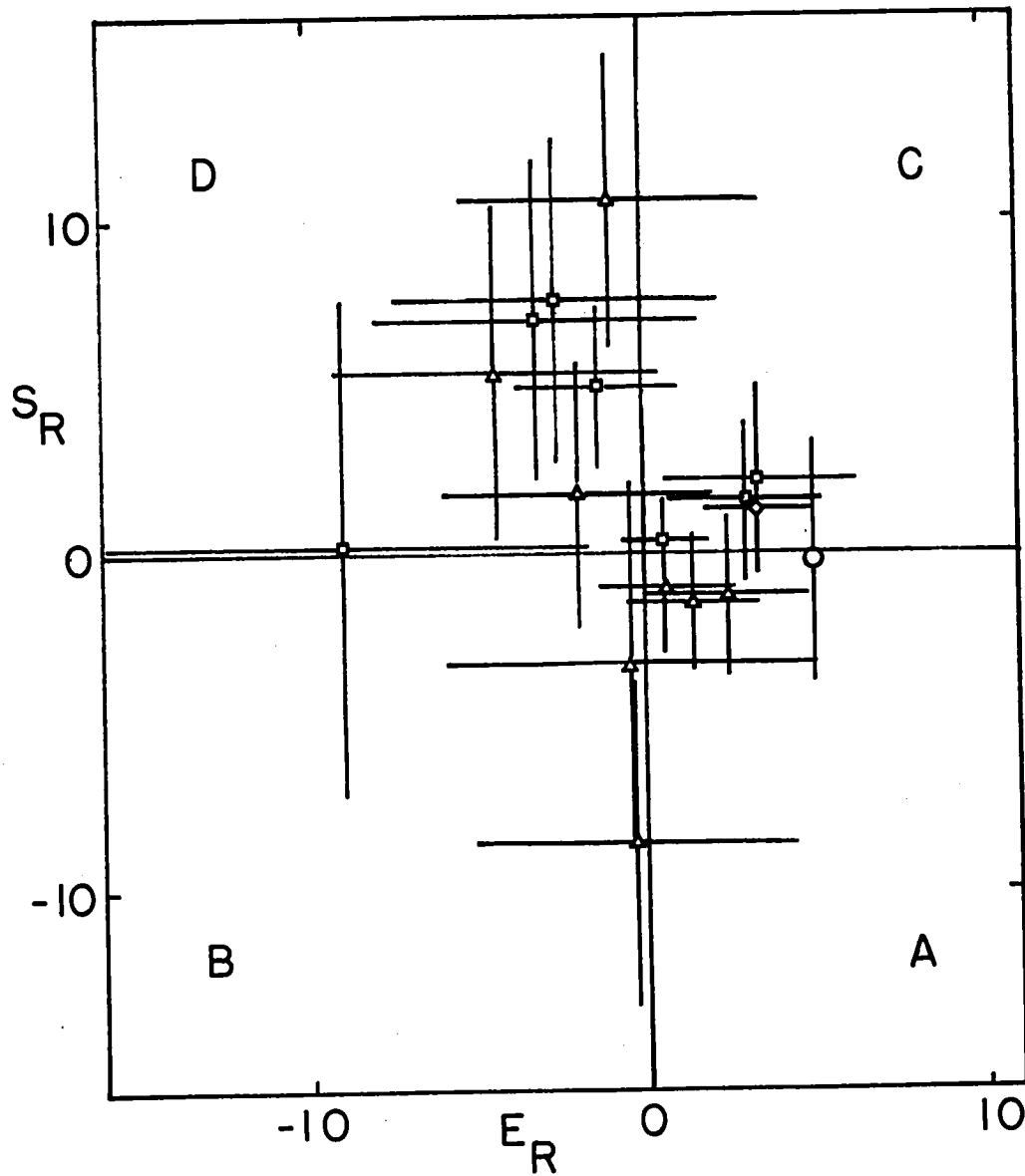


Figure 5. Coefficient ranges for  $S$  vs.  $\chi_1$ ; symbols and labelling of cases as in Figure 4.

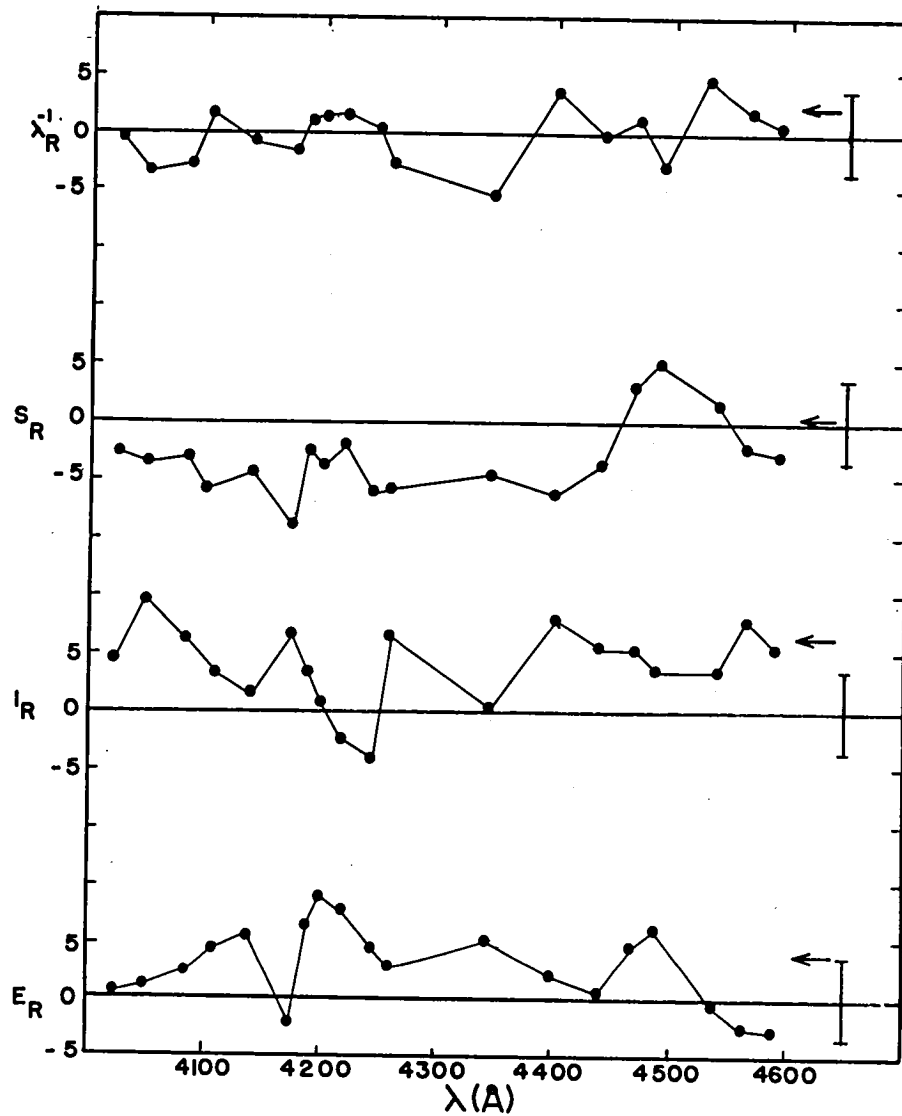


Figure 6. Running solution for S Car D895. The error bars represent  $\pm$ SD, the standard deviation of the observed velocities. The arrows indicate the coefficients for the fit for the entire plate. The positive  $\chi_i$  dependence is clearly supported by the running solution; the two points which are negative come from the two sets of ten lines containing  $\lambda 4226.73$  of CaI (2) which has an "anomalous" velocity of 288.8 km/s for its low ionization potential of 6.09 eV.

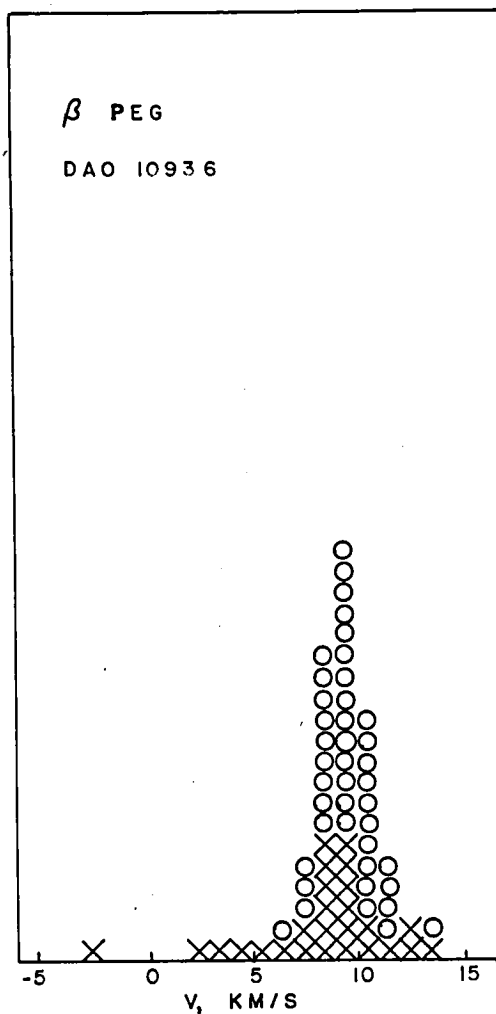


Figure 7. Heliocentric velocity histogram for  $\beta$  Peg. The mean absorption line velocity is 9.3 km/s. The larger scatter in the higher excitation lines may arise in part from misidentification of some lines as high excitation atomic lines rather than e.g. molecular features. Symbols for Figures 7-12: 0 = lines from 0-1 eV levels; X: 1-3 eV; +: >3 eV; II: absorption by ions; EII, Cr, Fe, H, etc. = emission lines.



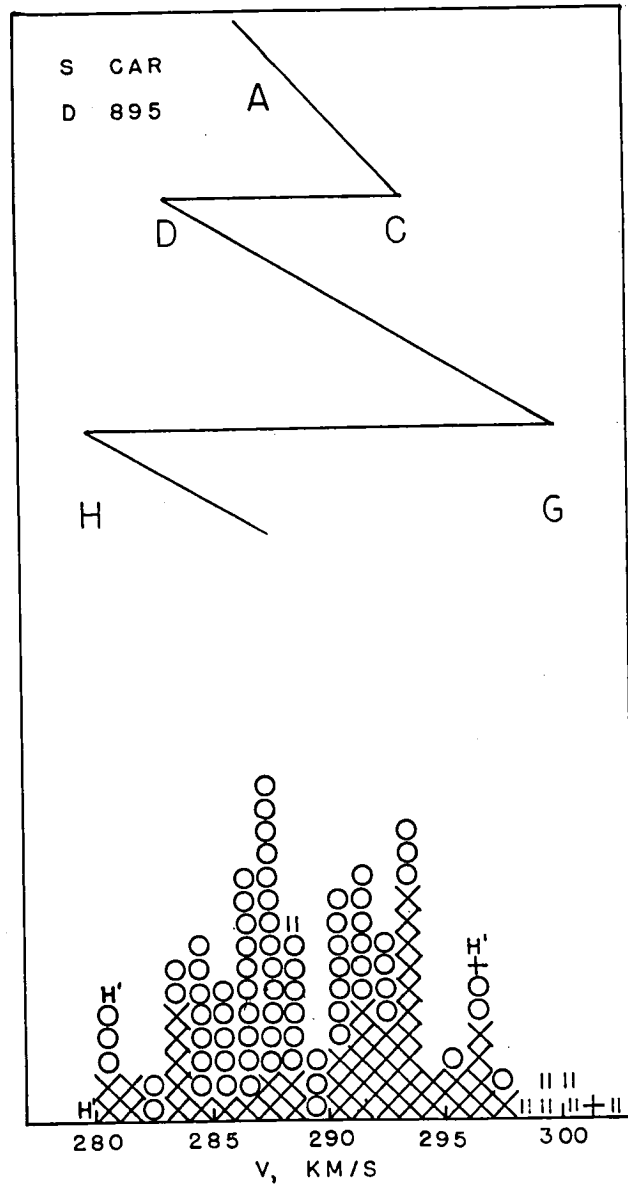


Figure 9. Heliocentric velocity histogram for S Car. Velocities as characterized by Figure 1 are indicated:  $A \approx 288$  km/s,  $C \approx 294$  km/s,  $G \approx 300$  km/s,  $D \approx 283$  km/s, and  $H \leq 280$  km/s.

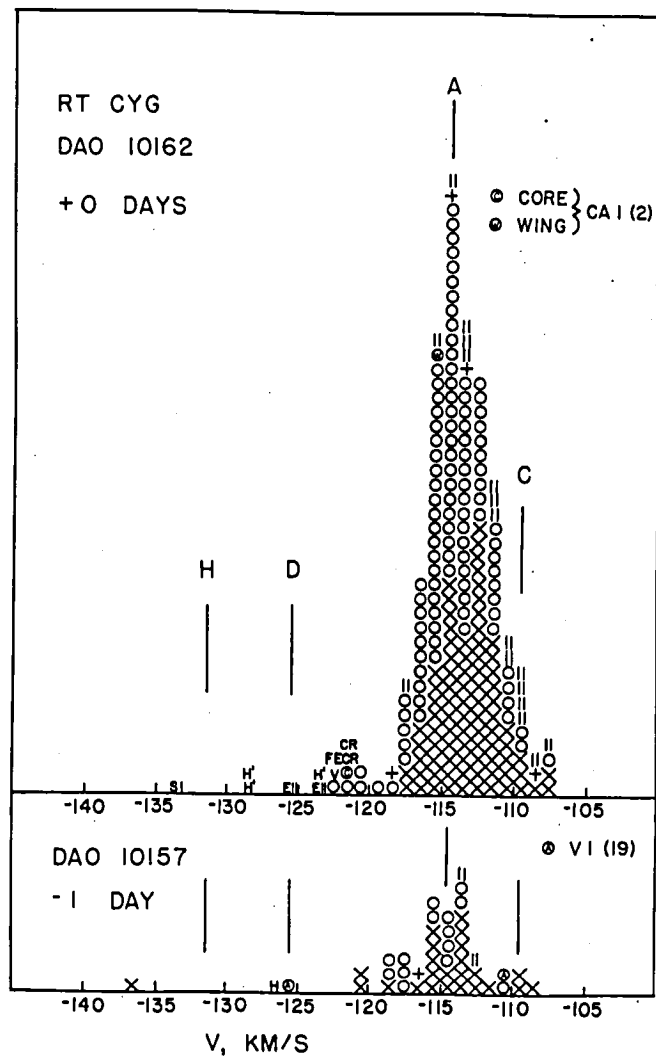


Figure 10. Velocity histogram for RT Cyg at maximum: DAO 10157 ( $\sim 6000 \text{ \AA}$ ) and DAO 10162 ( $\sim 4000 \text{ \AA}$ ). Assignment of velocities A (stellar), D (post shock), C (pre shock) and H (hydrogen emission) are noted as for Figures 8, 9. (There is an additional hydrogen emission line at  $-147 \text{ km/s}$  which is not shown.)

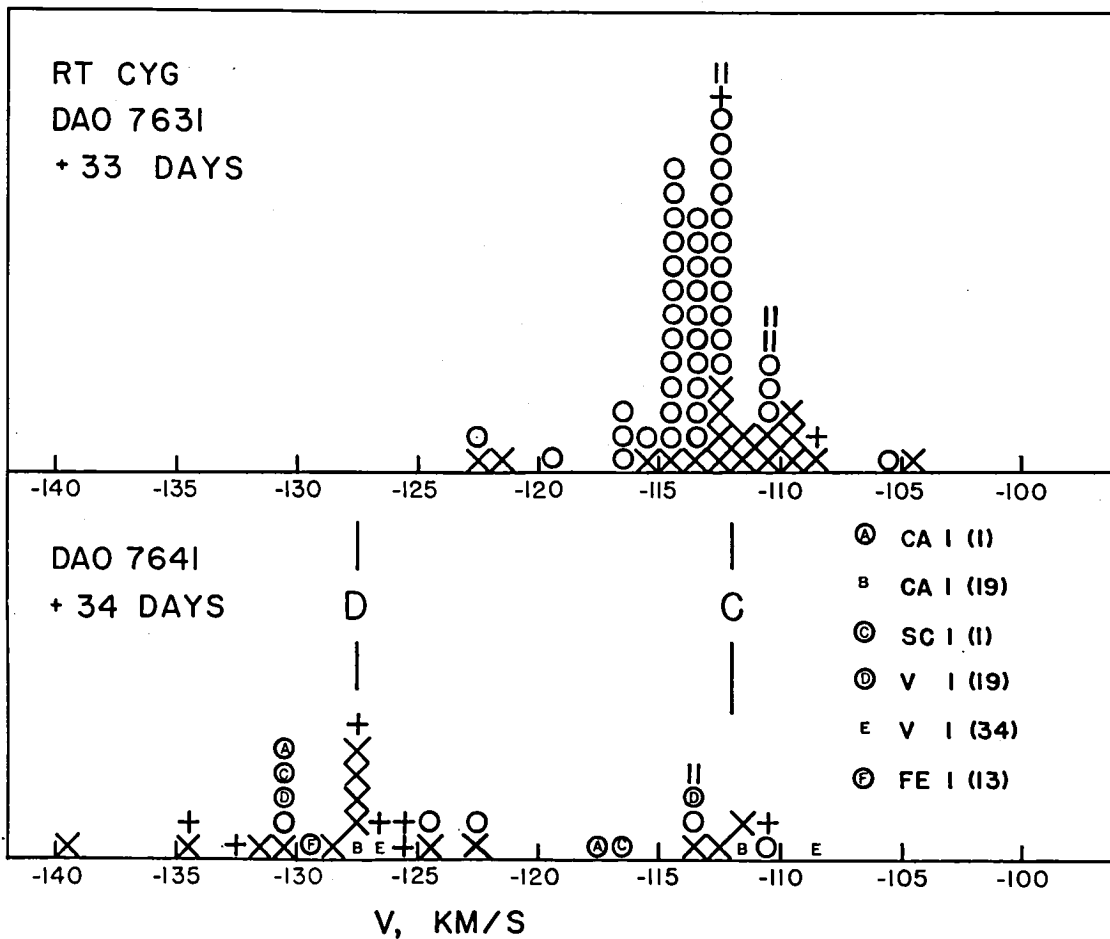


Figure 11. Velocity histograms for RT Cyg at +33/34<sup>d</sup>: DAO 7631 ( $\sim 4000 \text{ \AA}$ ) and 7641B ( $\sim 6000 \text{ \AA}$ , with components of doubled lines indicated).

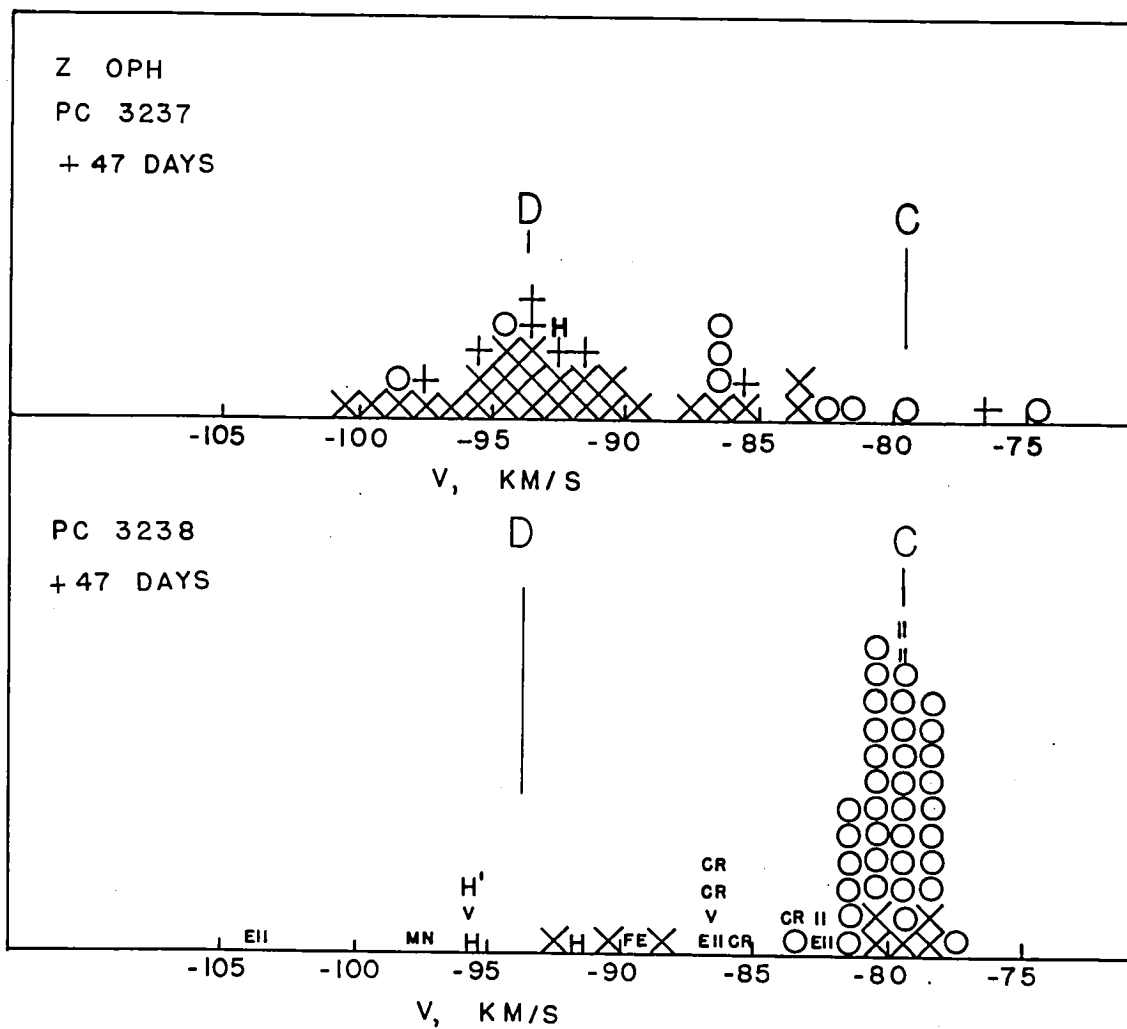


Figure 12. Velocity histogram for Z Oph at 47: PC 3237 (red) and 3238 (blue). The blue plate clearly indicates the pre-shock velocity C = -80 km/s; the red plate gives the post shock velocity D = -93 km/s.

Table 1. Allowed Coefficient Signs

Case	$X = 1/\lambda$	S	$\chi_i$	$\chi_e$	Position of reversing layer relative to source of excitation	Velocity gradient (outward velocity positive)
a	-	-	+	+	above	positive
b	-	-	-	-	below	positive
c	+	+	+	+	below	negative
d	+	+	-	-	above	negative

Table 2. Shock Model Interpretation of Regression Coefficients

Case	Region	Expected corollary behavior
a	above shock	<ul style="list-style-type: none"> <li>• mostly low excitation lines (<math>\leq 1</math> eV)</li> <li>• lines redshifted (<math>\leq 10</math> km/s)</li> <li>• higher excitation lines more redshifted</li> <li>• small scatter in velocity</li> </ul>
b	below shock	<ul style="list-style-type: none"> <li>• many higher excitation lines (<math>\geq 1</math> eV)</li> <li>• larger scatter than case a</li> <li>• lines at <math>v_*</math> to blueshifted (<math>\leq 5</math> km/s)</li> <li>• higher excitation lines more blueshifted</li> <li>• dependence on ionization potential</li> </ul>
c	c1. immediate post-shock region	<ul style="list-style-type: none"> <li>• very strong <math>\chi_i</math> dependence</li> <li>• moderate scatter</li> <li>• blueshift predominant</li> </ul>
	c2. Unresolved doubling and mixture of pre and post shock lines, especially high excitation lines	<ul style="list-style-type: none"> <li>• very large scatter</li> <li>• two velocities-favored in histograms</li> <li>• broad features and apparent blends at intermediate velocities</li> <li>• lines both redshifted and blueshifted compared to <math>v_*</math></li> <li>• exclusion of high excitation lines should convert case c2 to case a, with lower scatter.</li> </ul>
d	d1. immediate pre shock region	<ul style="list-style-type: none"> <li>• strong <math>\chi_e</math> and <math>\chi_i</math> dependence</li> <li>• small scatter</li> </ul>
	d2. unresolved doubling of low excitation lines	<ul style="list-style-type: none"> <li>• <math>\chi_e</math> dependence</li> <li>• large scatter</li> <li>• broad features and apparent blends</li> <li>• exclusion of low excitation lines converts d to b, with smaller scatter.</li> </ul>

Table 3. Results of the Regression Analysis

Plate <sup>(1)</sup>	Phase	$\lambda\lambda$	(n0-3eV)	$\langle v \rangle$	$\frac{n(1-3)}{n(0-3)}$	SD <sup>o</sup>	SD <sup>f</sup> /SD <sup>o</sup>	1/ $\lambda$	S	$\chi_1$	$\chi_e$	Case
$\beta$ Peg DAO 10936		4325-4606	63	9.3	.36	1.4	.97	-.7	-.4	-.1	-1.0	--
L <sup>2</sup> Pup D 888		3770-4427	89	53.2	.20	1.8	.88	+1.9	+1.4	-.5	+3.2	c
S Car D 895		3835-4693	106	291.7	.37	3.6	.67	+1.6	-.1	+6.3	+4.9	a,c
RT Cyg:												
DAO 10157	-1 <sup>d</sup>	5866-6599	36	-113.9	.64	2.4	.85	-1.2	-.6	+1.9	+2.5	a,c
DAO 10162	0 <sup>d</sup>	3797-4586	190	-113.6	.45	2.0	.89	+2.6	-1.4	-.6	+1.5	c,d
10157+10162			226	-113.7	.48	4.3	.93	+4.9	+.8	+.5	+.0	c,d
Pb 14597	+8 <sup>d</sup>	6141-6599	12	-111.1	.6	6.6	.88	-.1	-3.3	+8.0	-.5	a,c
Pb 14598	+8 <sup>d</sup>	7511-7714	3	-120.4	.3	7.9	--	--	--	--	--	--
14597+14598			15	-112.6	.5	7.0	.94	+2.6	-2.2	+2.3	-6.4	--
DAO 9345	+10 <sup>d</sup>	5866-6563	26	-136.7	.81	4.6	.59	+4.9	+10.7	-4.7	-1.0	d
DAO 9351	+11 <sup>d</sup>	5889-6678	55	-125.7	.80	3.9	.72	+3.2	+1.8	-6.4	+2.1	(d)
9345+9351			81	-129.2	.80	4.2	.72	+3.4	+5.2	-6.1	-2.1	d
DAO 7631	+33 <sup>d</sup>	4351-4722	55	-113.2	.29	2.0	.88	-2.9	-1.1	-1.1	+.6	a,b
DAO 7641A	+34 <sup>d</sup>	5889-6632	30	-125.1	.80	4.8	.83	+4.8	+5.3	-.9	-4.5	(d)
DAO 7641B	+34 <sup>d</sup>	6090-6613	20	-123.7	.63	4.9	.86	-4.1	-8.7	-5.6	-.4	b
7631+7641B			75	-116	.38	3.3	.94	-1.2	-2.0	-2.8	-2.5	--
Z Oph:												
Pc 10318	-8 <sup>d</sup>	3905-4482	22	-81.8	.30	2.3	.88	+.7	+.8	+1.3	+2.9	a,c
Pc 3184	+5 <sup>d</sup>	5857-6624	15	-86.4	.73	7.5	.81	+7.0	+0.2	+7.2	-8.9	c,d
EC 2688	+36 <sup>d</sup>	4861-6172	28	-87.5	.46	2.5	.74	-2.6	+5.0	+7.6	-1.4	c,a
Pc 7840	+44 <sup>d</sup>	3770-4496	42	-84.7	.19	2.8	.88	+2.7	+2.2	-2.7	+3.5	c,d
Pc 7846	+44 <sup>d</sup>	5426-6743	44	-88.5	.68	4.9	.82	-1.4	+7.0	-1.0	-3.2	c,d
7840+7846			86	-86.6	.44	4.4	.82	+5.3	+4.2	-2.9	-.6	c,d
Pc 3237	+47 <sup>d</sup>	5567-6707	30	-92.2	.83	4.8	.84	-2.4	+7.6	-1.0	-2.7	c,d
Pc 3238	+47 <sup>d</sup>	4156-4571	41	-79.9	.12	1.2	.95	+1.2	+.4	-.3	+.5	(a)
3237+3238			71	-85.1	.42	6.9	.46	+13.4	+2.8	-1.2	-3.7	d

(1) Plate coding and dispersions: DAO: Dominion Astrophysical Observatory 48"; blue plates 6 Å/mm, red plates 10 Å/mm.  
Pb: Hale Observatories 200"; 7 Å/mm. Pc: Hale Observatories 200"; blue plates 9 Å/mm, red plates 13.5 Å/mm.  
D: Cerro Tololo Interamerican Observatory 60"; blue plates 9 Å/mm. EC: Lick Observatory 120"; 16 Å/mm.

(2) Some high excitation lines split, with  $v = -113$  km/s,  $-127$  km/s

(3) 7641A treats all lines as single; 7641B resolves split lines with  $v = -128$  km/s,  $-113$  km/s.

(4) This plate contains several split lines and many broad ones.

Table 4. Properties of the four stars studied. Periods, mean spectral types, and maximum visual magnitudes from Clayton and Feast (1969) and Feast (1963); visual amplitudes from Campbell (1955) and Kukarkin *et al.*, GCVS; velocities and shock amplitudes from the present study. Both  $v_*$  and  $\Delta v$  are uncertain by  $\pm 3$  km/s.

	L <sup>2</sup> Pup	S Car	RT Cyg	Z Oph
Period	141 <sup>d</sup>	150 <sup>d</sup>	191 <sup>d</sup>	350 <sup>d</sup>
Spectral Type at maximum	M5e	M0e	M2e	K4ep
$m_v$ (mean max.)	2.6	5.7	7.3	8.1
$\Delta m_v$	3.4	2.7	4.5	4.0
$v_*$ , km/s	53	288	-113	-85
$\Delta v$ , km/s	17	{ 20 11 }	13-16	13-16

### Discussion

Belserene: Did you discuss the objectivity of your statistical criteria with a mathematician, perhaps?

Willson: That's a terrible question. I showed them to a mathematician. He made very little comment. It's a semi-empirical rule. I'm sure that there are mathematical arguments, but they depend on sample size, the reliability of the measurements, etc. Those parameters are so uncertain that the rule of thumb and iterative consistency seem to be pretty good for the first round. Actually, because so many cases turn out to be across the shock, I'm not sure that we learn too much from the coefficients themselves. I tend to like the histograms better, but we started off with the other part.